Spline driven: high accuracy projectors for tomographic reconstruction from few projections

Fabien Momey*, Loïc Denis, Catherine Burnier, Éric Thiébaut, Jean-Marie Becker, and Laurent Desbat

***Abstract*—Tomographic iterative reconstruction methods need a very thorough modeling of data. This point becomes critical when the number of available projections is limited. At the core of this issue is the projector design, i.e. the numerical model relating the representation of the object of interest to the projections on the detector.**

***Voxel driven* and *ray driven* projection models are widely used for their short execution time in spite of their coarse approximations. *Distance driven* model has an improved accuracy but makes strong approximations to project voxel basis functions. Cubic voxel basis functions are anisotropic, accurately modeling their projection is therefore computationally expensive. Smoother and more isotropic basis functions both better represent continuous functions and provide simpler projectors. These considerations have led to the development of spherically symmetric volume elements, called blobs. Set apart their isotropy, blobs are often considered too computationally expensive in practice.**

In this paper, we consider using separable B-splines as basis functions to represent the object and we propose to approximate the projection of these basis functions by a 2D separable model. When the degree of the B-splines increases, their isotropy improves and projections can be computed regardless of their orientation. The degree and the sampling of the B-splines can be chosen according to a trade-off between approximation quality and computational complexity.

We quantitatively measure the good accuracy of our model and compare it with other projectors like distance-driven and the model proposed by Long et al. [1]. From numerical experiments, we demonstrate that our projector with an improved accuracy better preserves the quality of the reconstruction as the number of projections decreases. Our projector with cubic B-splines requires about twice as many operations as a model based on voxel basis functions. Higher accuracy projectors can be used to improve the resolution of existing systems, or to reduce the number of projections required to reach a given resolution, potentially reducing the dose absorbed by the patient.

***Index Terms*—Tomography, Reconstruction, Inverse Problems, Signal processing, B-splines.**

EDICS: COI-TOM - Tomographic Imaging.

I. Introduction

ITERATIVE reconstruction methods for tomography have long proven their ability to enhance reconstruction quality, compared to the filtered backprojection (FBP) [2]. In PET/SPECT imaging where the signal-to-noise ratio is very poor, iterative methods are largely preferred. Iterative methods produce better reconstructions both because they consider a more realistic model of the underlying physics of positron annihilations and counting statistic, and because they can include powerful edge-preserving regularizations. Several works in the area of compressive sensing [3], [4] have shown that good quality reconstructions could be obtained even from a reduced set of projections thanks to regularization terms such as total variation. The drawback of iterative methods is however their computational time and FBP [5] is still the method of choice in X-ray computed tomography. Nevertheless ongoing researches on algorithms and continued increase of computational power, with multi-core processor units or GPU-based implementation facilities, call for a re-evaluation of the potential of iterative methods in this domain.

Iterative methods require a numerical model of the data acquisition process: the so-called *projector*. The projector is used for the reprojection of the current estimate of the object being reconstructed. These projections are then compared with the actual measurements at each iteration. A backprojection operator is also needed, which implements the adjoint of the projector. These operators naturally need to have fast implementations in order to obtain efficient reconstruction algorithms. To make the most out of the data, the projector must model accurately the physical process of data acquisition (the X-ray transform). When considering tomographic reconstruction from a limited number of projections, as in dynamic tomography, the accuracy of the projector and the choice of an adequate regularization become crucial.

We recently proposed in a conference paper an accurate projector based on separable B-splines [6]. These preliminary results showed that the proposed projector, called *spline driven*, could outperform the popular *distance driven* model in reconstruction quality, with a reasonable computational

This work was supported by the MiTiV project (Méthodes Inverses pour le Traitement en Imagerie du Vivant), funded by the French ANR (N° ANR-09-EMER-008).

Fabien Momey* was with the Université de Lyon, F-42023, Saint-Etienne, France; CNRS, UMR5516, Laboratoire Hubert Curien, F-42000, Saint-Etienne, France; Université de Saint-Etienne, Jean Monnet, F-42000, Saint-Etienne, France. He was also with the Université de Lyon, Lyon, F-69003, France; Université Lyon 1, Observatoire de Lyon, 9 avenue Charles André, Saint-Genis Laval, F-69230, France; CNRS, UMR 5574, Centre de Recherche Astrophysique de Lyon; École Normale Supérieure de Lyon, Lyon, F-69007, France. He is now with the Université Grenoble Alpes, F-38000 Grenoble, France; CEA, LETI, MINATEC Campus, F-38054 Grenoble, France (e-mail: fabien.momey@cea.fr).

Éric Thiébaut is with the Université de Lyon, Lyon, F-69003, France; Université Lyon 1, Observatoire de Lyon, 9 avenue Charles André, Saint-Genis Laval, F-69230, France; CNRS, UMR 5574, Centre de Recherche Astrophysique de Lyon; École Normale Supérieure de Lyon, Lyon, F-69007, France (e-mail: eric.thiebaut@univ-lyon1.fr).

Loïc Denis, Catherine Burnier and Jean-Marie Becker are with the Université de Lyon, F-42023, Saint-Etienne, France; CNRS, UMR5516, Laboratoire Hubert Curien, F-42000, Saint-Etienne, France; Université de Saint-Etienne, Jean Monnet, F-42000, Saint-Etienne, France (e-mail: loic.denis,catherine.burnier,jean-marie.becker@univ-st-etienne.fr).

Laurent Desbat is with the Université Grenoble Alpes, TIMC-IMAG, F-38000 Grenoble, France; CNRS, TIMC-IMAG, F-38000 Grenoble, France; CHU de Grenoble,TIMC-IMAG, F-38000 Grenoble, France (e-mail: laurent.desbat@imag.fr).

overhead. The present paper extends this preliminary study in the following ways:

- we provide a more detailed analysis of B-spline basis functions, especially their ability to approximate isotropic features (Sec. III and Fig. 1 to 3);
- we compare our projector to the improved method (compared to *distance driven*) of Long *et al.* [1] both by analyzing the errors of the footprint approximations of basis functions (Fig. 6 and 7) and by comparing reconstruction quality in fan beam geometry (Fig. 10);
- we show that the reconstruction quality can be maintained even when the number of projections is reduced thanks to the joint use of an accurate projector and an edge-preserving regularization (Fig. 9).

The paper is organized as follows. Section II introduces the reconstruction method and the role of the projector. Section III describes the proposed spline driven projector and compares it to other approaches. Reconstruction results are given in Section IV, where the influence of the number of projections is illustrated and reconstruction quality is compared to the state-of-the-art projector by Long *et al.* [1].

II. Tomographic projectors for iterative reconstruction

A. The direct model

The object of interest is the starting point of the projector used in iterative reconstruction. Let $f : \boldsymbol{x} \mapsto f(\boldsymbol{x})$ be the 3D function modeling the volume to be reconstructed and defined for all space coordinates $\boldsymbol{x} = (x, y, z) \in \mathbb{R}^3$. The function $f(\boldsymbol{x})$ is directly related to the attenuation of the X-rays by the object of interest (SI units: m^{-1}) and the observed intensity $I(\boldsymbol{u})$ follows from the physical principle of the Beer-Lambert law:

$$I(\boldsymbol{u}) = I_0 \, \exp\Big(-\int_{\boldsymbol{x}\in L(\boldsymbol{u})} f(\boldsymbol{x}) \, \mathrm{d}\boldsymbol{x}\Big) \tag{1}$$

with I_0 the intensity of the X-ray source and $L(\boldsymbol{u})$ the straight line from the X-ray source S to the position $\boldsymbol{u}$ on the detector.

A convenient parametric model of the object of interest consists in approximating $f(\boldsymbol{x})$ by a decomposition on a shift-invariant basis of functions $\varphi_k(\boldsymbol{x}) = \varphi(\boldsymbol{x} - \boldsymbol{x}_k)$:

$$f(\boldsymbol{x}) \approx \widetilde{f}(\boldsymbol{x}) = \sum_k c_k \, \varphi(\boldsymbol{x} - \boldsymbol{x}_k) \tag{2}$$

where $\varphi(\boldsymbol{x})$ is the kernel function of the basis and the 3D positions $\boldsymbol{x}_k = (x_k, y_k, z_k)^{\mathrm{T}} \in \mathbb{R}^3$ define a regularly spaced grid of N samples. The approximation $\widetilde{f}(\boldsymbol{x})$ of $f(\boldsymbol{x})$ in (2) is a 3D function characterized by the N-dimensional vector of coefficients:

$$\boldsymbol{c} = (c_1, c_2, \ldots, c_N)^{\mathrm{T}} \in \mathbb{R}^N \, . \tag{3}$$

The sampled object $f_k = \widetilde{f}(\boldsymbol{x}_k)$ (required for display and analysis) can be computed from the coefficients:

$$\boldsymbol{f} = \boldsymbol{\Phi} \cdot \boldsymbol{c} \tag{4}$$

where $\Phi_{k,k'} = \varphi(\boldsymbol{x}_k - \boldsymbol{x}_{k'})$ showing that the interpolation by $\boldsymbol{\Phi}$ is essentially a discrete convolution.

The projection of the object f for a given orientation of the tomographic system (positions of the source and the detector relative to the volume of interest), denoted by θ, is given by:

$$\widetilde{y}^\theta(\boldsymbol{u}) = \int_{\boldsymbol{x}\in L^\theta(\boldsymbol{u})} f(\boldsymbol{x}) \, \mathrm{d}\boldsymbol{x} = \sum_k c_k F_k^\theta(\boldsymbol{u}) \, , \tag{5}$$

where

$$F_k^\theta(\boldsymbol{u}) = \int_{\boldsymbol{x}\in L^\theta(\boldsymbol{u})} \varphi(\boldsymbol{x} - \boldsymbol{x}_k) \, \mathrm{d}\boldsymbol{x} \, , \tag{6}$$

is the so-called footprint of the k-th basis function. As a result the projector can be written as:

$$\widetilde{\boldsymbol{y}}^\theta = \mathbf{R}^\theta \cdot \boldsymbol{c} \quad \text{with} \quad R_{qk}^\theta = F_k^\theta(\boldsymbol{u}_q) \, , \tag{7}$$

where $\widetilde{\boldsymbol{y}}^\theta$ gathers the data model values $\widetilde{y}_q^\theta = \widetilde{y}^\theta(\boldsymbol{u}_q)$ at the position $\boldsymbol{u}_q$ of the q-th detector pixel.

B. Regularized reconstruction

The reconstruction amounts to seeking the coefficients $\boldsymbol{c}$ which minimize a criterion with the general form [7], [2]:

$$\begin{aligned} \boldsymbol{c}^+ &= \arg\min_{\boldsymbol{c}} \Big\{ \sum_\theta \mathcal{J}_{\mathsf{data}}^\theta(\widetilde{\boldsymbol{y}}^\theta \mid \boldsymbol{y}^\theta) + \mu \, \mathcal{J}_{\mathsf{prior}}(\boldsymbol{f}) \Big\} \\ &= \arg\min_{\boldsymbol{c}} \Big\{ \sum_\theta \mathcal{J}_{\mathsf{data}}^\theta(\mathbf{R}^\theta \cdot \boldsymbol{c} \mid \boldsymbol{y}^\theta) + \mu \, \mathcal{J}_{\mathsf{prior}}(\boldsymbol{\Phi} \cdot \boldsymbol{c}) \Big\} \, . \end{aligned} \tag{8}$$

In this criterion, $\mathcal{J}_{\mathsf{data}}^\theta$ is a data-fidelity term which ensures consistency of the model $\widetilde{\boldsymbol{y}}^\theta$ with the data $\boldsymbol{y}^\theta$. The term $\mathcal{J}_{\mathsf{prior}}$ accounts for prior information and is needed to regularize the inverse problem and avoid noise and artifacts amplifications. The hyperparameter μ controls the tradeoff between data fitting and regularity. Having a fast projector is critical because the minimization is performed by iterative methods.

C. State-of-the-art in tomographic projection

The choice of the basis function $\varphi(\boldsymbol{x})$ and the approximations made to compute its footprints $F_k^\theta(\boldsymbol{u})$ are essential for an accurate and fast modeling of the projections. A list of desirable properties of basis functions are:

i. Accurate modeling of the object $f(\boldsymbol{x})$ that preserves important object features such as sharp edges.
ii. Compact support for $\varphi(\boldsymbol{x})$ to ensure the sparsity of the resulting projector.
iii. Separability along spatial dimensions to reduce the computational burden by factorizing computations.
iv. Robustness to geometric transformations of the object (translation, rotation, magnification).
v. Spherical symmetry for isotropic projection.

Standard models such as *voxel driven* or *ray driven* [8] are based on raw samples which are linearly interpolated (either in the object space or in the data space) for the purpose of the projection. The coarse approximations made by such models give rise to strong artifacts in the reconstructed object unless a great deal of projections are used (typically several hundreds) to smooth out the consequences of the approximations.

Most existing models use cubic voxels as their basis functions. These functions are advantageous for being easy to manipulate and very compact as a given voxel does not spread over its neighbors. The *distance driven* projector [9] is based on such basis functions. This model projects the voxel's central section that is mostly parallel to the detector plane. Then the obtained quadrilateral footprint is approximated with a rectangle covering at best the delimited region. The overlapping areas on the impinged detector pixels are used to weight the voxel value, and thus calculate the contribution of the voxel to each pixel. Long *et al.* [1] proposed a much more accurate projection of a cubic voxel given by a separable footprint composed of trapezoidal functions. Their model is exact in parallel beam geometry.

The anisotropic behavior of cubic voxels contrasts with the isotropic nature of tomographic projection. The choice of isotropic basis functions has led to so-called "blobs" [10], [11], [12], [13], [14], improving the accuracy of the models of the object and its projections. In tomography, the Kaiser-Bessel function is a main representative of this class of functions. Ziegler *et al.* [15] developed a blob-based projector by precomputing the 2D footprint once for all.

III. The spline driven projector

A. Modeling the object

1) Approximation error: Given the basis of functions, the best coefficients c_k should minimize some measure $\|f-\widetilde{f}\|$ of the approximation error. In sampling theory [16], $\|f-\widetilde{f}\|$ is usually the L_2 norm and the optimal $\widetilde{f}$ is thus the orthogonal projection of f on the subspace spanned by the basis functions φ_k. The least approximation error ϵ_f only depends on the kernel function φ, on the sampling step Δ and, of course, on the object $f(\boldsymbol{x})$. In 1D, an expression of the least error for regular signals is [17], [18]:

$$\epsilon_f = \min_{\boldsymbol{c}} \|f-\widetilde{f}\|_2 \approx \left[\int_{-\infty}^{+\infty} E_\varphi(\omega\Delta)\,|\hat{f}(\omega)|^2\,\frac{\mathrm{d}\omega}{2\pi}\right]^{1/2} \tag{9}$$

where the hat denotes the Fourier transform and E_φ is the error kernel defined by:

$$E_\varphi(\omega) = 1 - \frac{|\hat{\varphi}(\omega)|^2}{\sum_{k\in\mathbb{Z}}|\hat{\varphi}(\omega+2\,k\,\pi)|^2}\,. \tag{10}$$

For a given sampling step, a good basis function should have a low least approximation error ϵ_f.

2) B-splines as basis functions: Splines of degree d are piecewise polynomial functions with degree at most d and continuously differentiable up to order $d-1$. Splines on a regular grid of samples can be written as a unique linear combination of a regularly shifted kernel. Such a kernel is itself piecewise polynomial and is called a B-spline [18].

Let β^d denote a B-spline of degree d. The B-spline of degree 0 is the rectangular pulse:

$$\beta^0(x) = \begin{cases} 1 & \text{if } |x| < 1/2; \\ 1/2 & \text{if } |x| = 1/2; \\ 0 & \text{otherwise;} \end{cases} \tag{11}$$

and the B-spline of higher degree are constructed by multiple convolutions of β^0:

$$\beta^d(x) = \underbrace{\beta^0 * \cdots * \beta^0}_{d+1 \text{ terms}}(x)\,. \tag{12}$$

With this notation and considering evenly spaced samples with a step Δ, a 1D spline of degree d writes:

$$s(x) = \sum_{k\in\mathbb{Z}} c_k\ \beta^d((x-x_k)/\Delta)\,. \tag{13}$$

For such 1D splines, the modeling error ϵ_f is $O(\Delta^{d+1})$ [16], [18], [19]. Hence using B-splines of higher degree decreases this error, or let one uses a coarser sampling rate for a given tolerance.

Going back to the formulation of the object representation in (2), we propose to use 3D separable B-splines of degree d as our basis functions:

$$\varphi(x,y,z) = \beta^d(x/\Delta)\beta^d(y/\Delta)\beta^d(z/\Delta)\,, \tag{14}$$

with Δ the sampling step of the grid. Taking B-splines of degree 0 yields nothing else than the cubic voxels which are the most compact B-splines. According to the central limit theorem and B-splines being d-fold convolutions of a rectangular pulse, they become closer to a Gaussian function as their degree d increases. Thus 3D separable B-splines tend to spherically symmetric functions, while preserving a compact support of size $(d+1)^3$. As a result, increasing the degree d not only yields an improved approximation error but also provides quasi-isotropic basis functions. These advantages are at the expense of an enlargement of the support of the basis functions and thus of an increase of the computational burden. However, as we will show, this additional cost is mitigated by the use of separable functions. The good properties of B-splines are related to the fact that they are the shortest and smoothest scaling functions for a given order of approximation [16]. More specifically, the cubic (degree 3) B-splines are members of the family of MOMS functions (Maximum Order Minimum Support), giving them a form of optimality in this context.

3) Comparison with the state-of-the-art basis functions: Fig. 1 shows the error kernels (10), in 1D, for B-splines from degree $d=0$ to 3, and for the ideal blob as defined by Matej & Lewitt [14]. The higher the degree of the B-spline, the faster the approximation error decreases below the Nyquist frequency when $\omega\times\Delta\to 0$, and tends to the optimality. Blobs also improve the quality of object modeling. We notice that the error kernel of the blob is very close to that of the quadratic B-spline (degree 2), although with a larger support.

Fig. 1 reveals that B-splines are much better basis functions for representing band-limited signals. Modeling sharp edges, *i.e.* not band-limited signals, is also one of the desired properties stated in section II-C. A typical anatomical feature of a human body in tomography is composed of tissues having different absorption levels; the object $f(\boldsymbol{x})$ to be reconstructed is therefore expected to have sharp transitions between areas with specific absorbing properties.

To estimate how B-splines of high degree compare to cubic voxels and blobs, we have represented the attenuation map

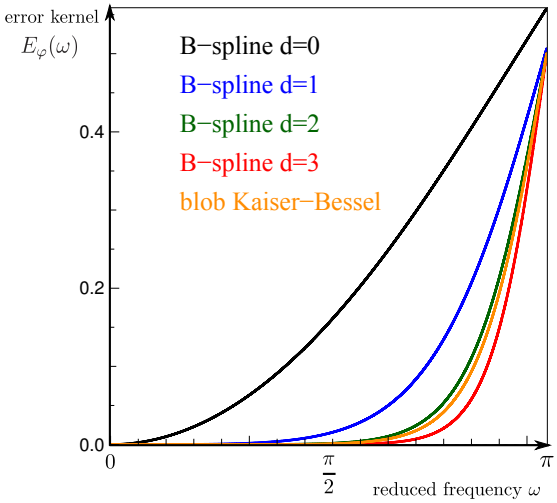

Fig. 1. Error kernels, as a function of the reduced frequency, of B-splines of different degrees d. For comparison, the error kernel of a Kaiser-Bessel blob with ideal parameters $m = 2$; $a = 2$; $\alpha = 10.4$ is plotted.

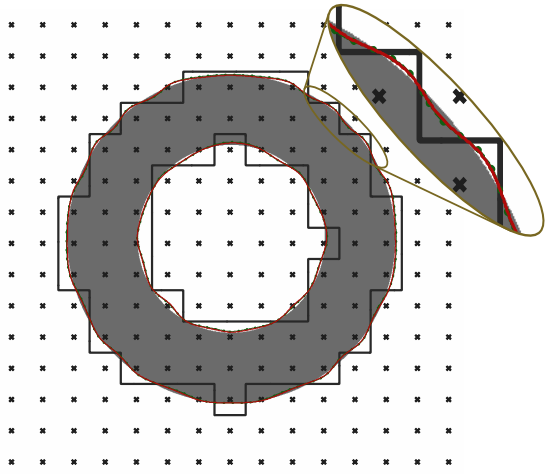

Fig. 2. Localization of the sharp edges found on thresholded approximations of a ring on a discrete 2D grid (crosses). The black curve corresponds to the cubic voxels' representation; the green curve with points corresponds to the blobs' representation; the red curve corresponds to the cubic B-splines' representation. (On this figure, the green and red contours are indiscernible. See Fig. 3 to discriminate them.)

of an absorbing ring with sharp edges on a regularly spaced 2D grid of basis functions' positions with a low resolution. The best representation, *i.e.* the model with coefficients $\boldsymbol{c}$ that minimize the approximation error $\|f - \widetilde{f}\|$, has been computed for three different kernel functions: cubic voxel, cubic B-spline ($d = 3$) and blobs. Then each model has been interpolated on a grid much finer than the sampling grid to draw the mid-height level curve. This contour is shown in Fig. 2 for each approximation. The more accurate localization of the sharp edges by both the cubic B-spline-based and the blob-based representations is unequivocal compared with the cubic voxel-based representation which shows a staircase boundary. This behavior evidences the critical lack of isotropy of cubic voxels. Conversely, for cubic B-splines and blobs, the boundaries are precisely localized whatever the orientation. We have also calculated the root mean squared error (RMS)

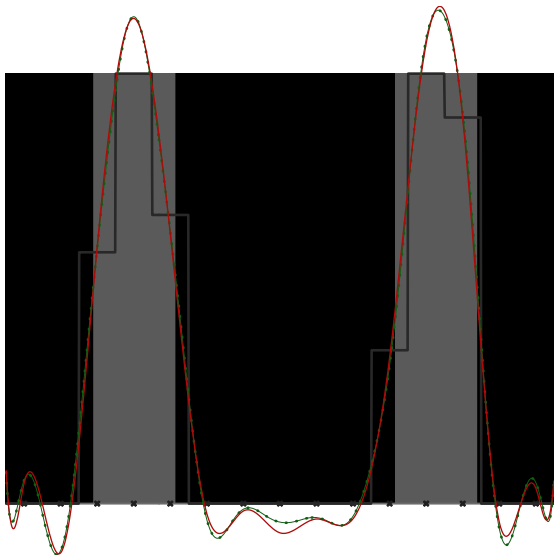

Fig. 3. 1D profile across the median horizontal line of the graph of Fig. 2. The black curve corresponds to the cubic voxels' representation; the green curve with points corresponds to the blobs' representation; the red curve corresponds to the cubic B-splines' representation.

and the edge localization error for every approximation. These errors for cubic voxels are respectively 16.8% and 6.4%. Blobs are 1.8 times better in RMS and 6.8 times better in localization error than cubic voxels, while cubic B-splines are the most accurate being 1.9 times better in RMS and 8.4 times better in localization error than cubic voxels. However, as shown by Fig. 3, Gibbs oscillations appear when modeling sharp edges with basis functions having a high approximation order. Such oscillations are visible for the cubic B-spline-based and the blob-based representations. Nevertheless, these side effects are low compared with the gain of isotropy and accuracy. Moreover, a suitable choice of regularization could help flattening the oscillations.

To model the kind of object we want to reconstruct, cubic voxels are thus not as suitable as more isotropic basis functions such as separable B-splines of higher degrees or blobs. In principle, lowering the approximation error of cubic voxels is possible by reducing significantly the sampling step but this increases the computational burden and the size of the reconstruction problem. Compared to separable B-splines, blobs are perfectly isotropic but are much more complex to handle and require more numerical operations. For instance, the computation of the sampled object $\boldsymbol{f}$ at every iteration of a regularized approach, see (4) and (8), can be computed very quickly for a B-spline based model by means of fast digital filtering operations [18], [20], [21].

B. Modeling the data

We consider a general tridimensional system (Fig. 4) where the object is static relatively to a 3D Cartesian frame with coordinates $\boldsymbol{x} = (x, y, z)$ evenly sampled at positions $\boldsymbol{x}_k$. We assume a flat detector and denote $\boldsymbol{u} = (u, v)$ the coordinates in the 2D Cartesian frame with axis aligned with the rows and the columns of the detector. Each projection is acquired with

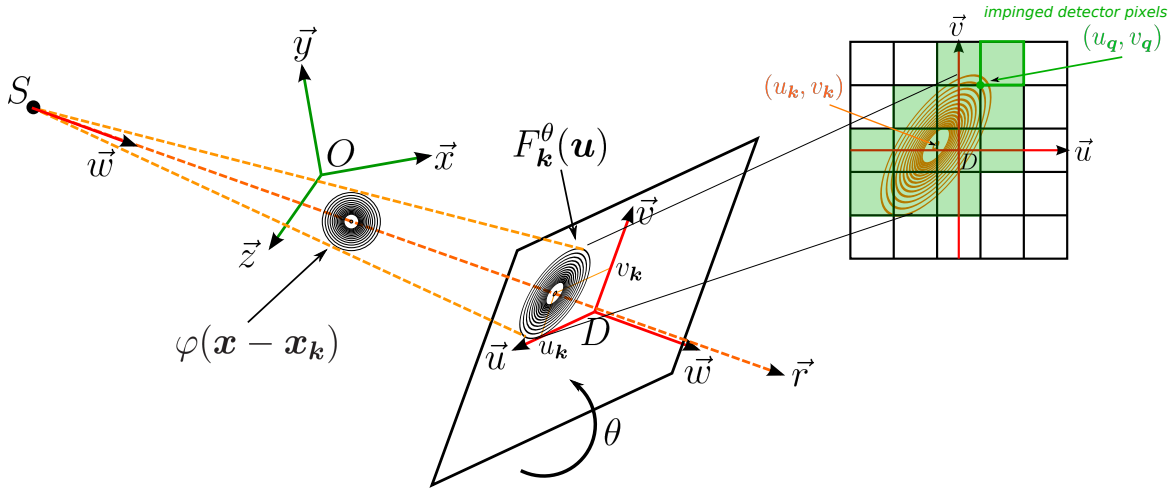

Fig. 4. Cone beam projection scheme of a basis function $\varphi(\boldsymbol{x} - \boldsymbol{x}_k)$ on the detector. θ denotes the orientation of the detector, rotating around the center O. The direction of the ray, starting from the source $S(\theta)$, orthogonal to the detector plane is identified by the vector $\vec{w}(\theta)$. The direction of the ray passing through the central position $\boldsymbol{x}_k = (x, y, z)$ of the k-th voxel is identified by the vector $\vec{r}$. The footprint of $\varphi(\boldsymbol{x} - \boldsymbol{x}_k)$ is denoted F_k^θ.

a given orientation denoted θ. The unit vector $\vec{w}$ defines the direction perpendicular to the detector and oriented from the source S to the detector.

To improve the data model, stated in (5) and (7), we also take into account pixel integration on the detector by defining the model for the q-th pixel at orientation θ as:

$$\begin{aligned} \widetilde{y}_q^\theta &= \iint \widetilde{y}^\theta(\boldsymbol{u})\, P_q(\boldsymbol{u}) \mathrm{d}^2\boldsymbol{u} \\ &= \sum_{k \in \Omega_q^\theta} \underbrace{\left(\iint F_k^\theta(\boldsymbol{u}) P_q(\boldsymbol{u}) \mathrm{d}^2\boldsymbol{u} \right)}_{R_{qk}} c_k \,, \end{aligned} \tag{15}$$

where $P_q : \boldsymbol{u} \mapsto P_q(\boldsymbol{u})$ is the response of the pixel and Ω_q^θ is the set of voxels k impinging this pixel. Equation (15) is a linearization of the Beer-Lambert law — integration of the X-ray transform instead of the photon flux (see 1). This approximation is valid in the case of low X-ray absorption. We assume that $P_q(\boldsymbol{u})$ is a 2D square pulse of dimensions $\Delta_{\mathsf{pix}} \times \Delta_{\mathsf{pix}}$ centered at the position $\boldsymbol{u}_q$ of the pixel. The pixel response is thus a separable shift-invariant function: $P_q(\boldsymbol{u}) = \beta^0((u - u_q)/\Delta_{\mathsf{pix}})\beta^0((v - v_q)/\Delta_{\mathsf{pix}})$ with β^0 given by (11).

1) Footprint in parallel beam geometry: In parallel beam geometry, all integration lines are aligned with $\vec{w}(\theta)$. We approximate the footprint of a voxel $\boldsymbol{\beta}_k^d$ by a 2D B-spline of same degree d separable along the detector axis:

$$F_k^\theta(\boldsymbol{u}) = \beta^d((u - u_k^\theta)/\Delta)\, \beta^d((v - v_k^\theta)/\Delta) \tag{16}$$

where $(u_k^\theta, v_k^\theta) = \boldsymbol{u}_k^\theta$ is the projection on the detector along the rays of the position $\boldsymbol{x}_k$ of the k-th voxel for orientation θ. Expression (16) is exact when the direction $\vec{w}(\theta)$ of the parallel beam projection is aligned with one of the axis $\vec{x}$, $\vec{y}$, or $\vec{z}$; it is only an approximation for other orientations. However the higher the degree d the better this approximation.

Thanks to the quasi-isotropy property of B-splines of sufficient degree, the footprint in our *spline driven* model (*cf.* section III-A2) has approximately the same shape whatever the orientation θ.

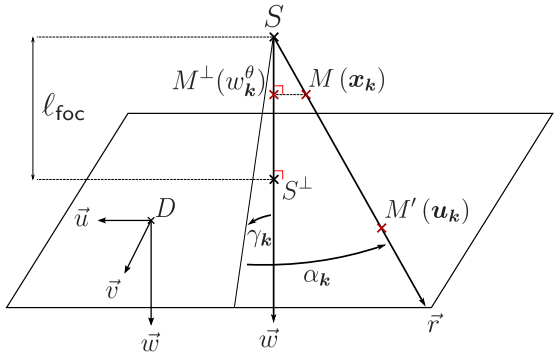

Fig. 5. Scaling parameters in cone beam geometry. ℓ_{foc} is the focal length of the system (distance between the source point S and its orthogonal projection $S^\perp$ on the detector). $M(\boldsymbol{x}_k)$ is the center of the basis function $\boldsymbol{\beta}_k^d$. Its cone beam projection on the detector is the point $M'(\boldsymbol{u}_k^\theta)$. $M^\perp(w_k^\theta)$ is the orthogonal projection of M on the straight line $\{S, \vec{w}\}$. Its position w_k is used to determine the magnification factor Γ_k^θ. α_k and γ_k are angles with respect to directions $\vec{u}$ and $\vec{v}$.

2) Footprint in cone beam geometry: In the case of cone beam geometry, the magnification and the distortion, both depending on the position of the voxel in the field of view, has to be taken into account (see Fig. 5). In order to keep the separability property of the footprint on the detector, we approximate these effects by scaling factors applied to the footprint in (16), such that:

$$F_k^\theta(\boldsymbol{u}) = \beta^d((\eta_k^\theta\, u - u_k^\theta)/\Delta)\, \beta^d((\rho_k^\theta\, v - v_k^\theta)/\Delta) \tag{17}$$

with (see Fig. 5):

$$\eta_k^\theta = \frac{\cos\alpha_k}{\Gamma_k^\theta}\,, \quad \rho_k^\theta = \frac{\cos\gamma_k}{\Gamma_k^\theta}\,, \quad \Gamma_k^\theta = \frac{\ell_{\mathsf{foc}}}{w_k^\theta}\,, \tag{18}$$

η_k^θ and ρ_k^θ are distortion factors, Γ_k^θ is the magnification.

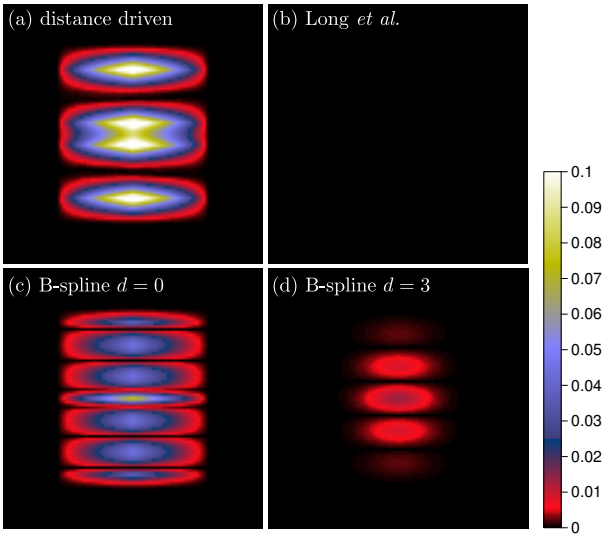

Fig. 6. Approximation errors in parallel beam geometry for footprints convolved by the pixel detector response. The projectors are: (a) *spline driven*, (b) the model of Long *et al.* SF-TT-A1, (c) and (d) our *spline driven* model. Models (a–c) are with cubic voxels, that is B-splines of degree $d = 0$; while model (d) is with B-splines of degree $d = 3$. The error maps show the absolute difference between the exact and the model-approximated footprints (assuming the same voxel shape). The detector rotates around the $\vec{z}$-axis. The worst case is considered here with the detector tilted by 45° with respect to the horizontal plane. Numerical values of the errors are: (a) EMAX $\simeq$ 12.3% (maximum error) and RMS $\simeq$ 2.4% (root mean square error); (b) EMAX $\simeq$ 0% and RMS $\simeq$ 0%; (c) EMAX $\simeq$ 7% and RMS $\simeq$ 1.3%; (d) EMAX $\simeq$ 1.3% and RMS $\simeq$ 0.2%.

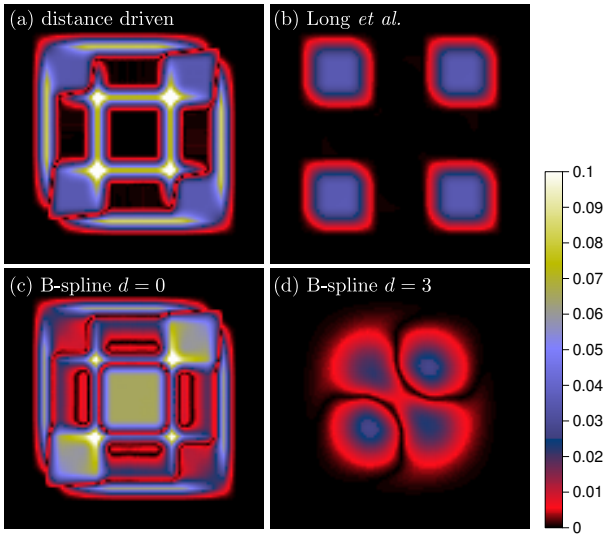

Fig. 7. Approximation errors in cone beam geometry for footprints convolved by the pixel detector response. The models are as in Fig. 6 but adapted to the cone beam geometry. The worst case is considered here: the detector is tilted by 0° with respect to the horizontal plane but the projected voxel is very off-centered (100mm, -150mm, 100mm). Numerical values of the errors are: (a) EMAX $\simeq$ 14.5% and RMS $\simeq$ 2.7%; (b) EMAX $\simeq$ 3.5% and RMS $\simeq$ 1.1%; (c) EMAX $\simeq$ 13.5% and RMS $\simeq$ 2.7%; (d) EMAX $\simeq$ 2.8% and RMS $\simeq$ 0.6%.

3) Approximation errors of the models: We quantified errors caused by our approximations for the footprints of *spline driven* and compared them with the *distance driven* and Long *et al.* projectors. For a given basis function and a given model, we calculated its exact and approximated footprints. We considered a tomographic system with a focal length ℓ_{foc} of 949mm, a source to rotation center distance of 514mm, and a flat detector with a pixel size of $1 \times 1\text{mm}^2$. This is the same configuration as in the article of Long *et al.* [1] in the study of their own approximated footprint's errors. For the Long *et al.* projector, we have implemented the particular SF-TT-A1 method as proposed in [1]. For the determination of the exact footprint at a given orientation of the detector, we used a Monte Carlo method consisting in calculating about 5×10^6 random lines of response (LOR) passing through the basis function. Each exact LOR was calculated by Romberg numerical integration [22]. The LORs approximated by each considered model were computed using their analytical expressions. Finally, we numerically computed the convolution of the footprints by the detector pixel response by summing the LOR included in the support of the pixel centered at each position of a 100×100 regular grid.

Fig. 6 displays the worst case errors caused by our approximations using B-splines with degree $d = 0$ and $d = 3$, compared with the *distance driven* and Long *et al.* approximated footprints' errors, in parallel beam geometry. Our projector is much more accurate than *distance driven*. In this geometry, the Long *et al.* model's approximation errors can only be caused by numerical rounding errors and are thus negligible.

In this comparison, we did not consider B-splines of degree higher than 3 because we have shown in [6] that using higher degree basis functions does not reduce the error by more than a factor of 2 while significantly increasing the computational burden (*cf.* section III-B4). B-splines of degree 3 appear to be a good trade-off between accuracy and computation time.

Fig. 7 shows the approximation errors in cone beam geometry. Compared to Fig. 6, errors are amplified due to approximations made to cope with the geometrical effects (magnification, off-axis distortions). In this configuration, *spline driven* is more accurate than both *distance driven* and Long *et al.* models, provided that the degree of the B-splines is sufficiently high.

Similarly to Fig. 3 in the paper [1], Fig. 8 compares the maximum approximation error for a centered voxel and an off-centered voxel as a function of the angles of projection, for several projectors: *distance driven*, Long *et al.* SF-TT-A1 and *spline driven* with $d = 3$. It can be observed that Long *et al.* model is the most accurate for a voxel at the center of the tomographic system. In the case (b) of a voxel farther from the system center, approximation errors are lower at all angles with the proposed *spline driven* projector. The worse error is about 10^{-2} with *spline driven*, 10^{-1} with the projector of Long *et al.*, and between 10^{-1} and 1 with *distance driven*.

Compared to blob-based projectors, our *spline driven* model is only approximately isotropic but requires much less numerical operations because it uses separable functions for its voxels and their footprints. In the next paragraph we show that the computational burden of our *spline driven* model is competitive with that of simpler approaches such as *distance driven* or Long *et al.*.

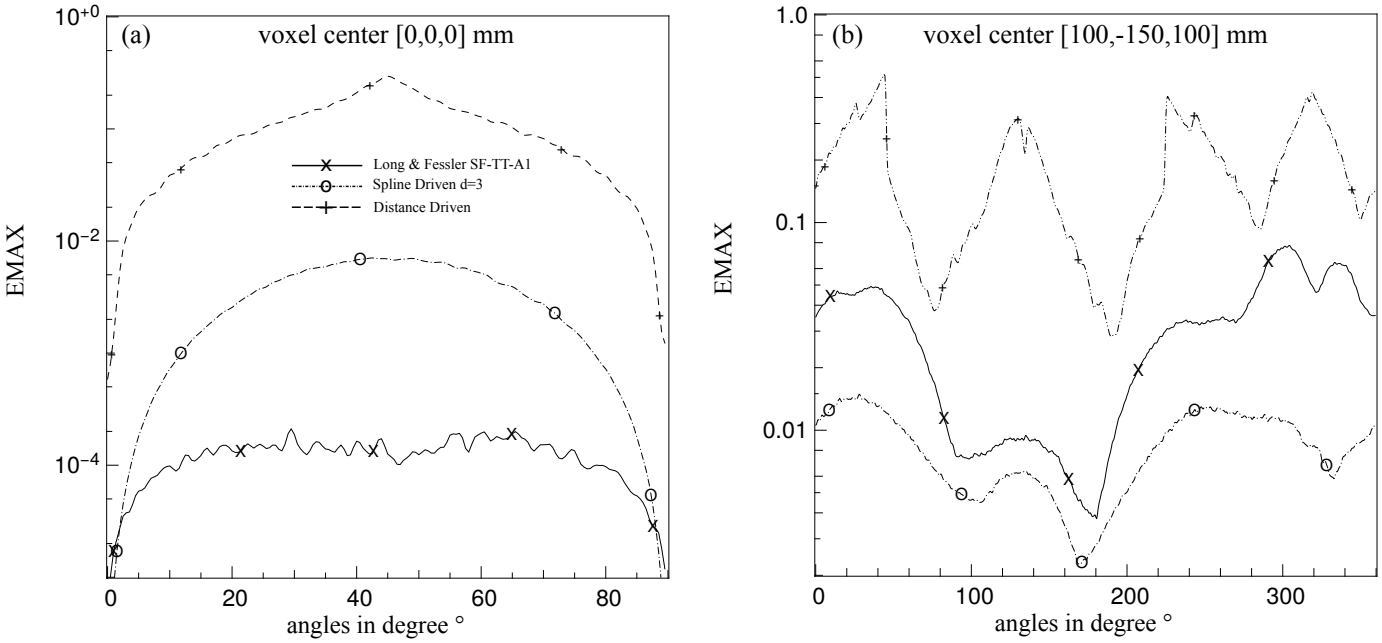

Fig. 8. Maximum approximation errors EMAX in cone beam geometry as a function of the angle of projection for *distance driven*, Long *et al.* SF-TT-A1 and *spline driven* with $d = 3$. (a) Voxel positioned at (0mm,0mm,0mm) from 0 to 90° (180 angles). (b) Voxel positioned at (100mm,-150mm,100mm) from 0 to 360° (720 angles). This figure is similar to Fig. 3 found in [1].

4) Computational burden: Spline driven increases the number of operations necessary to calculate the data values y_q^θ (15), due to the larger footprint of a given voxel. Cubic B-splines provide a good tradeoff between accuracy and computational burden. Let us consider a system where the voxels and detector pixels sampling rates are approximately equal. The width of the degree d B-spline support is $s = d+1$ in each direction. Its footprint impinges $(s+1)\times(s+1) = (d+2)\times(d+2)$ detector pixels in general. If we compare a cubic voxel ($d = 0$) with a cubic B-spline ($d = 3$), the number of impinged detector pixels for a given voxel is only multiplied by a factor between 2 and 3 in each direction. As the footprint considered in *spline driven* is still separable, the amount of operations is multiplied by the same factor, which remains competitive. Moreover our projection scheme, as well as the cubic voxel-based approaches, are easily parallelizable.

In the next section we analyze the improvements brought by *spline driven* projector in the context of reconstruction from a limited number of projections.

IV. Results on 2D fan beam reconstructions

A. Reducing the number of projections

In section III-A2, we claimed that the increase of accuracy due to the use of B-splines to model the object and its projections could reduce the amount of data required for a given reconstruction quality. Figure 9 displays reconstructions of a 2D Shepp-Logan phantom with our *spline driven* model and for a variable number of fan beam projections. We consider a circular source trajectory around the object with a fixed relative position of the detector with respect to the source. The object of interest has a size of 256×256 pixels and the projections are acquired by a detector with 512 pixels. The sampling step is the same for the object and for the detector. Note that, to avoid the so-called *inverse crime* [23], [24], an exact direct model (*i.e.* with no approximations except rounding errors) is used to compute the projections for simulating the data. Avoiding *inverse crime* is critical to assess whether modeling approximations can impair the reconstruction quality with undesirable artifacts.

The voxel coefficients $\boldsymbol{c}$ are reconstructed from the dataset $\left\{\boldsymbol{y}^\theta \;\middle|\; \theta \in \Theta\right\}$, with Θ the set of projection angles, by minimizing the criterion (8). The data-fidelity term is:

$$\mathcal{J}_{\mathsf{data}}(\boldsymbol{c}) = \sum_{\theta\in\Theta} \left\| \widetilde{\boldsymbol{y}}^\theta(\boldsymbol{c}) - \boldsymbol{y}^\theta \right\|_2^2 . \tag{19}$$

In order to preserve sharp edges in the sampled object $\boldsymbol{f} = \boldsymbol{\Phi}\cdot\boldsymbol{c}$, we choose a relaxed total variation (TV) prior [25] for the regularization:

$$\mathcal{J}_{\mathsf{prior}}(\boldsymbol{f}) = \sum_k \sqrt{\|\nabla_k \cdot \boldsymbol{f}\|_2^2 + \epsilon^2} . \tag{20}$$

with $\epsilon > 0$ a relaxation parameter and ∇_k a finite difference operator approximating the spatial gradient at position k. The minimization of (8) is carried out by the VMLM algorithm [27], a limited memory quasi-Newton method.

These results clearly show that the quality of the reconstruction is acceptable up to ~ 40 projections. This is an order of magnitude lower than the usual hundreds of projections required by standard reconstruction algorithms, particularly FBP. Note that, in contrast to some results presented in the literature, we avoided committing an *inverse crime* by using an accurate simulation of the projection to generate the data. Improving the quality of reconstruction from a limited number of projections opens the possibility to reduce the X-ray dose delivered to the patient for data acquisition. The quality of

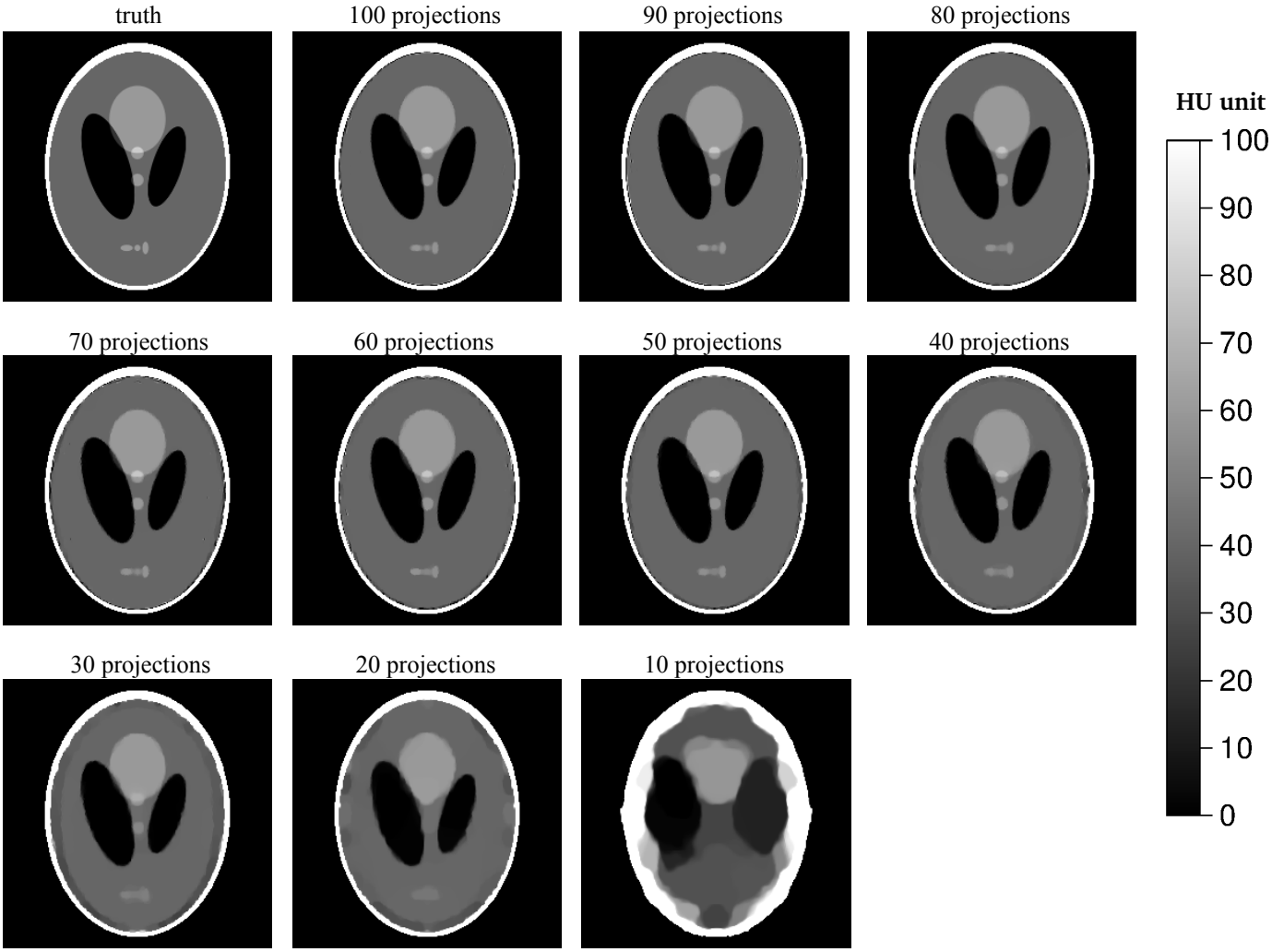

Fig. 9. Reconstructions of a 256×256 grid of a Shepp-Logan phantom with our *spline driven* projector using cubic B-splines, from a decreasing number of projections.

reconstruction observed here is also due to the TV regularizer which is very well suited to the reconstruction of piecewise constant objects [4]. In the following tests, we use reduced datasets of 60 projections.

B. Comparison of spline and Long et al. *models*

We compare *spline driven* and Long *et al.* on simulated projections of the two-dimensional Shepp-Logan phantom in fan beam geometry. The system and the acquisition protocol is the same as described in section IV-A. As we work in 2D, the particular implementation of the Long *et al.* projector is the SF-TR-A3 method as proposed in [1]. Again, to avoid committing an *inverse crime*, exact projections are computed for data simulation. From the simulated projections, we create two different datasets adding an uniform independent Gaussian noise approximately corresponding to a non-attenuated X-ray flux of respectively 9×10^7 (N1), and 9×10^6 (N2) photons per detector pixel per projection. This corresponds to variances of noise of respectively 1.11×10^{-8} for N1 and 1.11×10^{-7} for N2. For each noise level, we simulate 5 different random realizations of the noise. For the two considered models, the voxel coefficients $\boldsymbol{c}$ are reconstructed from a set of 60 noisy projections $\left\{\boldsymbol{y}^\theta \;\middle|\; \theta \in \Theta\right\}$ by minimizing the criterion (8). Since the noise is independent and Gaussian, the data-fidelity term is also given by (19). For the regularization, we still use the relaxed TV prior in (20).

Fig. 10 displays the reconstructions of 1 realization of the noise level N1, with two magnified regions of interest (ROI), where we also plot horizontal and vertical line profiles. For each projector, we use the regularization level μ which leads to the lowest RMS error in the blue ROI, *i.e.* the region where the finest details are expected (*cf.* Fig. 11). Selecting the best parameter with respect to the RMS computed on the whole image would have over-smoothed the smallest structures. The best reconstruction with our *spline driven* projector (in third column of Fig. 10) recovers most of the features without noticeable artifacts in spite of the low number of projections (60). Comparatively, the best reconstruction with the Long *et al.* projector (in the second column of Fig. 10) recovers less accurately the finest details, especially in the blue ROI. The reconstruction quality would improve if the number of projections available for the reconstruction increased, and all details

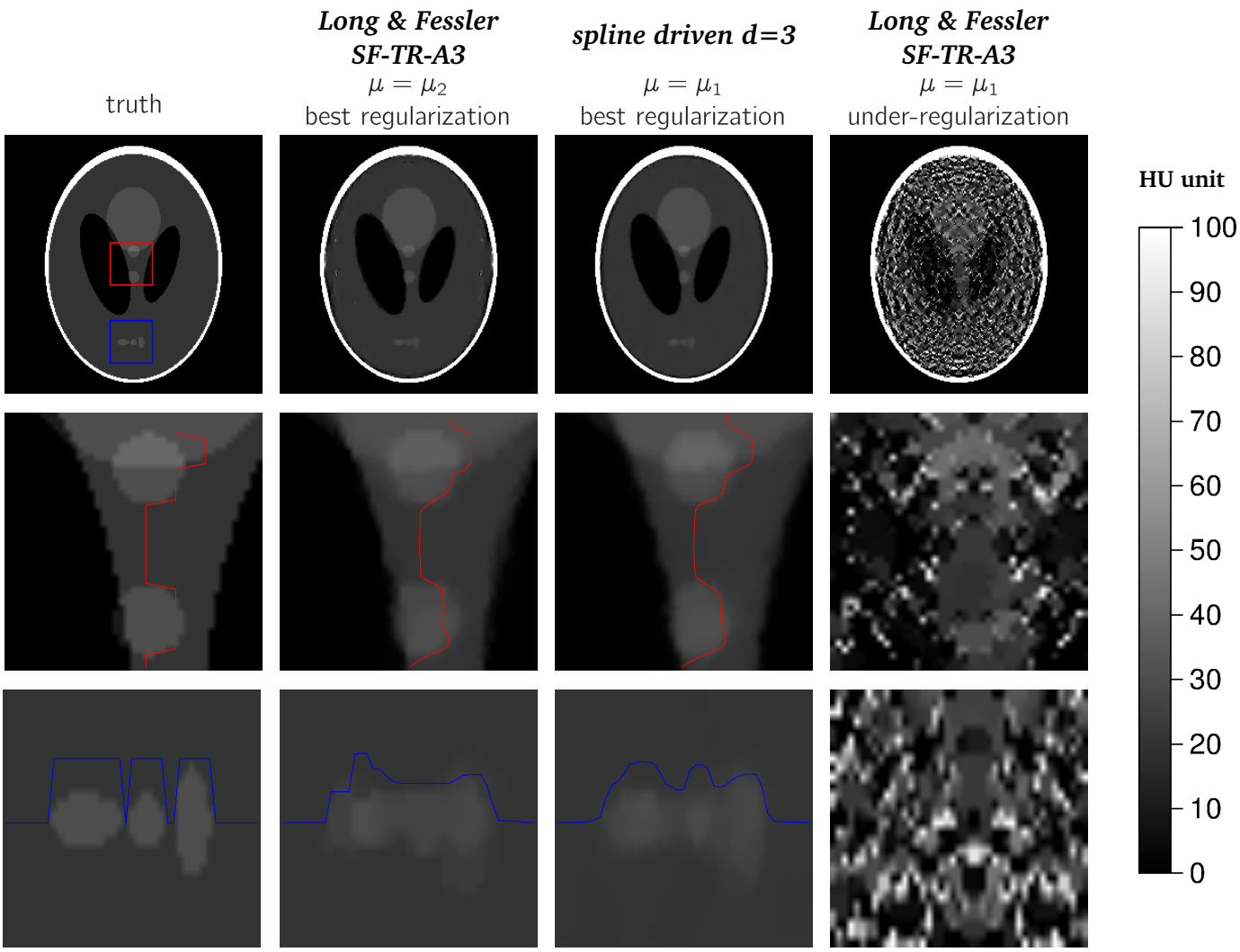

Fig. 10. Reconstructions of 1 realization of the noise level N1 of the 256×256 Shepp-Logan phantom, from a set of 60 fan beam projections with 512 detector pixels, with both the *spline driven* projector using cubic B-splines and the Long *et al.* SF-TR-A3 projector. The first column illustrates the true object. The first row shows the whole objects while the second and third rows are magnified views of the two squares drawn on the first image. The blue and red curves are line profiles along the horizontal and vertical directions. The second column shows the best achievable reconstruction with Long *et al.* projector ($\mu_2 = 9 \times 10^{-10}$). The third column corresponds to the best reconstruction with the proposed *spline driven* projector ($\mu_1 = 10^{-12}$). The fourth column shows the reconstruction with Long *et al.* projector if the same regularisation level as for *spline driven* is used, resulting here in an under-regularized reconstruction. The reconstructions with *spline driven* took a maximum of 3.5 times longer than with Long *et al.*.

would correctly be recovered with several hundred projections. The better reconstruction quality with *spline driven* is achieved at a lower regularization level ($\mu_1 = 10^{-12}$) than with *Long et al.* ($\mu_2 = 9 \times 10^{-10}$), which indicates a smaller modelization noise requiring less smoothing by the regularization term. If the same low regularization level is used with Long *et al.* projector, a very noisy under-regularized reconstruction is obtained (last column).

These qualitative results illustrate that using an accurate projector model is essential when dealing with a limited number of projections. The accuracy of the model has a direct impact on the quality of the restored object but also on the minimal amount of measurements needed to achieve satisfying reconstructions. The effect of using a coarser model can be mitigated if many projections are available and the regularization weight is increased, at the expense of a decrease of spatial resolution, to limit reconstruction artifacts.

In terms of computation time, these reconstructions took a maximum of 3.5 times longer than with Long *et al.*. So it is a bit more than the estimated computational burden (*cf.* section III-B4).

The curves in Fig. 11 indicate the RMS error in the two ROIs (identified by their colors in Fig. 11) as a function of the regularization level μ, for the mean reconstructed objects over the 5 realizations, and for the 2 noise levels N1 (a) and N2 (b). Whatever the ROI and the projector, the RMS curve appears to be convex; thus the best reconstruction is obtained for a unique optimal value of μ. Visual assessment (see Fig. 10) confirms that the RMS error computed in well chosen regions of interest is an appropriate metric to evaluate the quality of a reconstructed object. Besides, in any ROI, the optimal RMS error is always lower with our *spline driven* projector than with the Long *et al.* one up to a factor 1.2 (20% lower). This is a quantitative assessment of the improved reconstruction quality

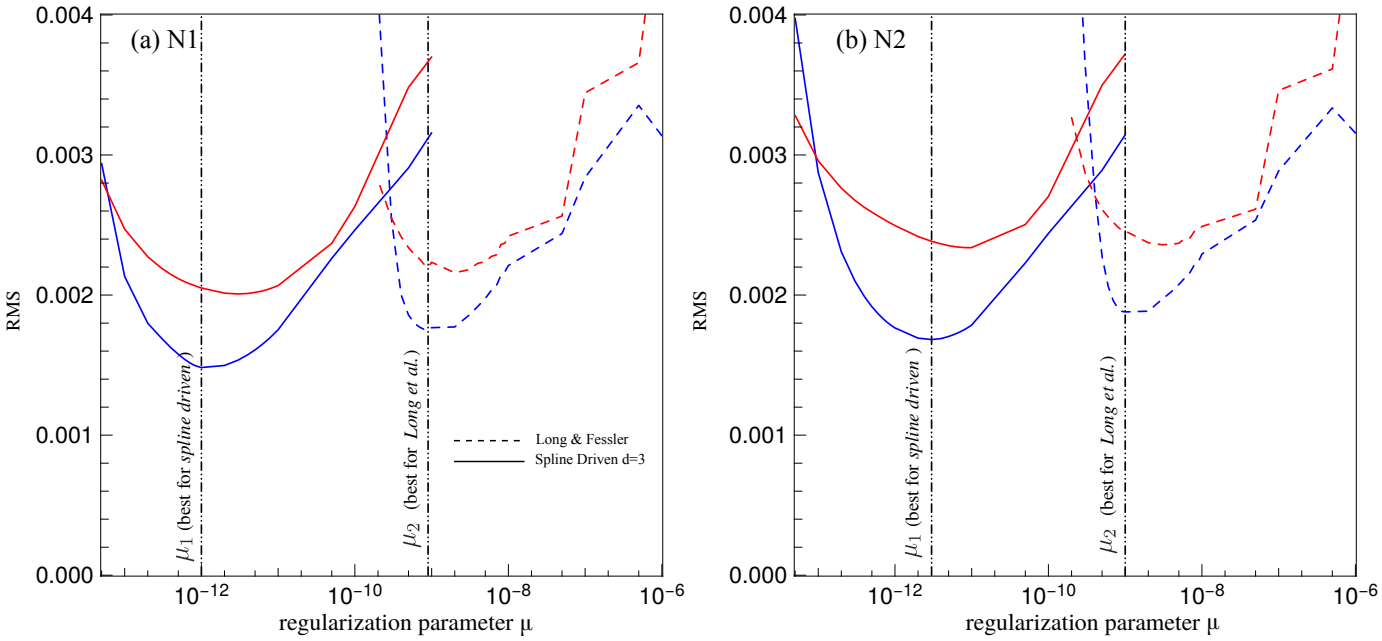

Fig. 11. Root mean squared error in the two ROIs (see Fig. 10) of the reconstructed object, normalized by the maximum value in the ROI, for various values of the hyperparameter μ (logarithmic scale). The RMS error is calculated from the mean reconstructed objects over the 5 realizations, respectively for the 2 noise levels N1 (variance 1.11×10^{-8}) (a) and N2 (variance 1.11×10^{-7}) (b). The solid curves correspond to reconstructions with the *spline driven* projector, and the dashed curves correspond to reconstructions with the Long *et al.* projector.

with our projector.

V. Conclusions

This paper describes the *spline driven* projector for iterative reconstruction. This projector achieves a good trade-off between accuracy and computational complexity. By exploiting a more accurate direct model compared to current models such as Long *et al.*, the quality of the restored object is enhanced and the number of projections necessary to achieve a given reconstruction quality is reduced. Thus, diagnoses can potentially be more easily established and the dose of radiation received by the patient be reduced.

Our approach exploits the good properties of B-spline basis functions to model the object of interest, to approximate its projections, and to account for pixel integration. Using separable 3D B-spline of degree 3, our basis functions are close to isotropic which is a clear improvement compared to cubic voxels. To achieve a fast projector, we also introduce a separable 2D approximation of the footprint for various beam geometries (parallel, fan beam and cone beam). Our model is less isotropic than blobs, but is separable and more compact, and is thus much faster to compute. The computational complexity of our model is only 2 to 3 times that of *distance driven* or Long *et al.* [1] models. While Long *et al.* [1] projector appears as the method of choice in parallel beam geometry, in cone-beam or fan-beam geometry the factor two computational overhead introduced by *spline driven* (with cubic B-splines) is compensated by the gain in accuracy. This improved accuracy becomes crucial when the number of projections is limited.

On the basis of numerical simulations, we have shown that by using a more accurate projection model we can achieve better reconstructions, even from a very limited number of projections (typically 5 to 10 times less than the number of projections typically used with filtered back-projections). This opens the possibility to reduce the X-ray dose delivered to the patient during data acquisition.

In a companion paper which has just been submitted, we exploit our *spline driven* model to produce spatio-temporal reconstructions on both simulated and empirical data. In this 3D+t context, the ability to achieve acceptable reconstructions from a much reduced number of projections is a strong requirement. Indeed, due to motion, only a very limited number of projections can be used to reconstruct the object at a given time.

References

[1] Y. Long, J.A. Fessler and J.M. Balter. *3D Forward and Back-Projection for X-Ray CT Using Separable Footprints*. IEEE Transactions on Medical Imaging, vol. 29, no. 11, pp. 1839-1850, 2010.

[2] J.A. Fessler. *Iterative methods for image reconstruction*. IEEE International Symposium on Biomedical Imaging Tutorial, Arlington Virginia, 2006.

[3] E.J. Candès, J. Romberg and T. Tao. *Robust uncertainty principles: exact signal reconstruction from highly incomplete frequency information*. IEEE Transactions on Information Theory, vol. 52, no. 2, pp. 489-509, 2006.

[4] G. Chen, J. Tang and S. Leng. *Prior image constrained compressed sensing (PICCS): A method to accurately reconstruct dynamic CT images from highly undersampled projection data sets*. Medical Physics, vol. 35, no. 2, pp. 660-663, 2008.

[5] M. Slaney and A. Kak. *Principles of computerized tomographic imaging*. SIAM, Philadelphia, 1988.

[6] F. Momey, L. Denis, C. Burnier, É. Thiébaut, J.-M. Becker and L. Desbat *A new representation and projection model for tomography, based on separable B-splines*. Proceedings of the IEEE Nuclear Science Symposium and Medical Imaging Conference, pp. 2602-2609, 2011.

[7] É. Thiébaut, *Introduction to Image Reconstruction and Inverse Problems*, in *Optics in Astrophysics*, R. Foy & F.-C. Foy (Eds.), NATO ASI Series **198**, pp. 397-422 Springer (Amsterdam), 2005.

[8] P.M. Joseph. *An improved algorithm for reprojecting rays through pixel images*. IEEE Transactions on Medical Imaging, vol. 1, no. 3, pp. 192-196, 1982.

[9] B. DeMan and S. Basu. *Distance driven projection and backprojection in three dimensions*. Physics in Medicine and Biology, vol. 49, no. 11, pp. 2463, 2004.

[10] R.M. Lewitt. *Multidimensional digital image representations using generalized Kaiser-Bessel window functions*. JOSA A, vol. 7, no. 10, pp. 1834-1846, 1990.

[11] R.M. Lewitt. *Alternatives to voxels for image representation in iterative reconstruction algorithms*. Physics in Medicine and Biology, vol. 37, no. 3, pp. 705, 1992.

[12] S. Matej and R.M. Lewitt. *Image representation and tomographic reconstruction using spherically symmetric volume elements*. Proceedings of the IEEE Nuclear Science Symposium and Medical Imaging Conference, vol. 2, pp. 1191-1193, 1992.

[13] S. Matej and R.M. Lewitt. *Efficient 3D grids for image reconstruction using spherically-symmetric volume elements*. IEEE Transactions on Medical Imaging, vol. 42, no. 4, pp. 1361-1370, 1995.

[14] S. Matej and R.M. Lewitt. *Practical considerations for 3D image reconstruction using spherically symmetric volume elements*. IEEE Transactions on Medical Imaging, vol. 15, no. 1, pp. 68-78, 1996.

[15] A. Ziegler, T. Köhler, T. Nielsen and R. Proksa. *Efficient projection and backprojection scheme for spherically symmetric basis functions in divergent beam geometry* Medical Physics, vol. 33, no. 12, pp. 4653-4663, 2006.

[16] M. Unser. *Sampling-50 years after Shannon*. Proceedings of the IEEE, vol. 88, no. 4, pp. 569-587, 2000.

[17] T. Blu and M. Unser. *Approximation error of quasi-interpolators and (multi-)wavelet expansions* Applied and Computational Harmonic Analysis, vol. 6, no. 2, pp. 219-252, 1999.

[18] M. Unser. *Splines: A perfect fit for signal and image processing*. IEEE Signal Processing Magazine, vol. 16, no. 6, pp. 22-38, 1999.

[19] P. Thévenaz, T. Blu and M. Unser. *Interpolation Revisited*. IEEE Transactions on Medical Imaging, vol. 19, no. 7, pp. 739-758, 2000.

[20] M. Unser, A. Aldroubi and M. Eden. *B-spline signal processing: Part I-Theory*. IEEE Transactions on Signal Processing, vol. 41, no. 2, pp. 821-833, 1993.

[21] M. Unser, A. Aldroubi and M. Eden. *B-spline signal processing: Part II-Efficient design and applications*. IEEE Transactions on Signal Processing, vol. 41, no. 2, pp. 834-848, 1993.

[22] W. Romberg *Vereinfachte numerische integration* Norske Vid. Selsk. Forh.(Trondheim), vol. 28, no. 7, pp. 30-36, 1955.

[23] J. Kaipio and E. Somersalo. *Statistical inverse problems: discretization, model reduction and inverse crimes*. Journal of Computational and Applied Mathematics, vol. 198, no. 2, pp. 493-504, 2007.

[24] A. Wirgin *The inverse crime* arXiv Mathematical Physics, 2004.

[25] L.I. Rudin, S. Osher and E. Fatemi. *Nonlinear total variation based noise removal algorithms*. Physica D: Nonlinear Phenomena, vol. 60, no. 1, pp. 259-268, 1992.

[26] S. Horbelt, M. Liebling and M. Unser. *Discretization of the Radon transform and of its inverse by spline convolutions*. IEEE Transactions on medical imaging, vol. 21, no. 4, pp. 363-376, 2002.

[27] J. Nocedal. *Updating quasi-Newton matrices with limited storage*. Mathematics of computation, vol. 35, no. 151, pp. 773-782, 1980.

Fabien Momey received the Engineer degree from École Supérieure de Chimie Physique Électronique de Lyon (CPE-Lyon), Lyon, France, in 2008 and the Ph.D. degree from Université Jean Monnet, Saint-Étienne, France, in 2013.

He is currently a Post-Doctoral Researcher at CEA-LETI, Université Grenoble Alpes, Grenoble, France, since september 2013. His research fields are signal and image processing for biomedical imaging. His areas of expertise are inverse problems resolution, image reconstruction for tomography and digital holography.

Loïc Denis received the Engineer degree from CPE-Lyon in 2003 and the Ph.D. degree from Université Jean Monnet, Saint-Étienne, France, in 2006.

He is currently an Assistant Professor with Télécom Saint-Étienne, Université Jean Monnet, Saint-Étienne. His research interests include image denoising and reconstruction, radar image processing, deconvolution, and digital holography.

Catherine Burnier received the Engineer degree from ICPI (former name of CPE-Lyon) in 1994 and the Ph.D. degree from Université Joseph Fourier, Grenoble, France, in 1997.

She is currently an Assistant Professor at the Laboratoire Hubert Curien, Université Jean Monnet, Saint-Étienne. She is teaching at CPE-Lyon. Her research topics are inverse problems, image reconstruction and calibration for tomography.

Éric Thiébaut graduated from École Normale Supérieure in 1987 and received the Ph.D. degree in astrophysics from Université Pierre et Marie Curie de Paris VII, Paris, France, in 1994.

Since 1995, he is an Astronomer at the Centre de Recherche Astrophysique de Lyon, France. His main interests are in the fields of signal processing and image reconstruction. He has made various contributions in blind deconvolution, optical interferometry, and optimal detection.

Jean-Marie Becker has a Ph.D. and Habilitation degree in image processing from Université Jean Monnet, Saint-Étienne, France.

He is currently Professor in CPE-Lyon. His research is centered on mathematical methods for image processing.

Laurent Desbat received the Ph.D. degree from Université Joseph Fourier, Grenoble, France, in 1990.

He is currently a Professor at the TIMC-IMAG, Université Grenoble Alpes, Grenoble, France. His main research topics are inverse problems, image reconstruction and calibration for tomography.